A Pandas complex adapted for piRNA-guided transposon silencing

Kang Zhao[#1], Sha Cheng[#2], Na Miao[#1], Ping Xu[#1,3], Xiaohua Lu[#1], Ming Wang[1], Yuhan Zhang[2], Xun Yuan[2], Weiwei Liu[1], Xin Lu[1], Xuan Ouyang[1], Peng Zhou[1], Jiaqi Gu[1,4], Yiqun Zhang[1], Ding Qiu[1], Shan Wang[1], Zhaohui Jin[2], Youzhong Wan[3], Jinbiao Ma[4], Ying Huang[2,5], Yang Yu[1,5]

[1]Institute of Biophysics, Key Laboratory of RNA Biology, Chinese Academy of Sciences, University of Chinese Academy of Sciences, Beijing, China, 100101
[2]State Key Laboratory of Molecular Biology, Shanghai Key Laboratory of Molecular Andrology, CAS Center for Excellence in Molecular Cell Science, Shanghai Institute of Biochemistry and Cell Biology, Chinese Academy of Sciences, University of Chinese Academy of Sciences, Shanghai, China, 200031
[3]School of Life Sciences, National Engineering Laboratory of AIDS Vaccine, Key Laboratory for Molecular Enzymology and Engineering of Ministry of Education, Jilin University, Changchun, Jilin, China, 130012
[4]State Key Laboratory of Genetic Engineering, Department of Biochemistry, School of Life Sciences, Fudan University, Shanghai, China, 200438

[#]contributed equally

[5]correspondence: yuyang@ibp.ac.cn; huangy@sibcb.ac.cn

Keywords: piRNA, transposon silencing, dNxf2, Panoramix, crystal structure, *Drosophila*, dNxf1/TAP, dNxt1/p15

Abstract

The repression of transposons by the Piwi-interacting RNA (piRNA) pathway is essential to protect animal germ cells. In *Drosophila* ovaries, Panoramix (Panx) enforces transcriptional silencing by binding to the target-engaged Piwi-piRNA complex, although the precise mechanisms by which this occur remain elusive. Here, we show that Panx functions together with a germline specific paralogue of a nuclear export factor, dNxf2, and its cofactor dNxt1 (p15) as a ternary complex to suppress transposon expression. Structural and functional analysis demonstrate that dNxf2 plays critical roles in Panx association via its UBA domain, and transposon silencing through binding to transposon transcripts directly. Furthermore, dNxf2 interacts with dNxf1 (TAP), which, unexpectedly, is also required for Panx-mediated silencing. Therefore, we propose that dNxf2 may function as a Pandas (Panoramix-dNxf2 dependent TAP/p15 silencing) complex, which counteracts the canonical RNA exporting machinery (TAP/p15) and restricts transposons to nuclear peripheries.

To maintain eukaryotic genome integrity, nascent transcripts of transposons are often targeted by nuclear Argonaute proteins for transcriptional gene silencing (TGS)(*1-5*). In animal gonads, the PIWI-clade Argonautes guided by piRNAs (PIWI-interacting RNA) are thought to recognize nascent transposon transcripts and direct sequence-specific heterochromatin formation(*3*). As a critical cofactor of *Drosophila* nuclear Piwi, Panoramix (Panx, also known as Silencio) links the target-engaged Piwi-piRNA complex to the general silencing machinery(*6*, *7*). Enforced tethering of Panx to nascent transcripts leads to cotranscriptional silencing and correlates with deposition of histone H3 lysine 9 trimethylation (H3K9me3) marks(*6*, *7*). However, the mechanism by which Panx mediates the repression remains unknown.

We cross-examined proteins that co-immunoprecipitated with Panx (fig. S1A) with piRNA pathway candidate genes from RNA interference (RNAi) screens(*8-11*). Unexpectedly, we identified dNxf2 as a potential cofactor of Panx (fig. S1A-C). dNxf2 belongs to an evolutionarily conserved NXF (nuclear export factor) family of proteins, yet depletion of dNxf2 had no effect on polyadenylated mRNA export(*12*, *13*). Instead, dNxf2 and its cofactor dNxt1 (also known as p15) were both identified in two published RNAi screens as being essential for transposon silencing(*8*, *9*). Similar to Panx, dNxf2 is specifically expressed in female gonads (fig. S1D).

To validate the interaction between Panx and dNxf2, we performed GFP immunoprecipitation from ovaries expressing GFP-Panx fusion under its native promoter. Results of mass spectrometry analysis (fig. S1B) and western blotting demonstrated that endogenous dNxf2 is associated with Panx (Fig. 1A). Likewise, Halo-tagged dNxf2 was able to precipitate endogenous Panx proteins from Ovarian Somatic Cell (OSC) lysates (Fig. 1B). We next tested if dNxf2 is functionally required for Panx-mediated silencing. The luciferase transcripts with BoxB sites in their 3′ untranslated regions are repressed if λN-Panx is tethered(*6*, *7*). The luciferase expression was then measured

upon germline-specific knockdowns of dNxf2 or dNxt1 (Fig. 1C). Despite λN-Panx tethering, loss of either dNxf2 or dNxt1 significantly weakened the ability of Panx to repress the reporter, as compared to the controls (Zuc or attp2, Fig. 1C). Consistent with the reporter de-repression, transposon transcripts are elevated upon dNxf2 RNAi (fig. S1E). Taken together, our data suggests that dNxf2 and dNxt1 may function as a heterodimer either with or downstream of Panx to suppress transposon expression.

Next, we used RNA sequencing (RNA-seq) to examine global effects on transposon expression with germline-specific knockdowns of dNxf2, compared with Panx RNAi (Fig. 1D-F). As expected, dNxf2 knockdown triggered a dramatic increase of transposon transcripts (Fig. 1D). The effect is similar to that of Panx (Fig. 1E-F), suggesting that dNxf2 is specifically required for silencing of transposons repressed by Panx. To rule out off-target effects of RNAi, we generated mutants of dNxf2 using CRISPR/Cas9 (fig. S2A)(*14*). Although the mutation we isolated removed just 20 amino acids from the N-terminus of dNxf2, mutant female flies were sterile (fig. S2B), similar to other core piRNA pathway mutants(*6*). Loss of dNxf2 had essentially no effect on Piwi nuclear localization or stability (fig. S2C-D), consistent with dNxf2's function as an effector protein. Furthermore, dNxf2 mutants showed global up-regulation of transposons (fig. S2E-G) and de-repression of the luciferase reporter despite λN-Panx tethering (fig. S3A). We noticed here that the endogenous Panx protein level is significantly reduced in the absence of dNxf2 (fig. S2D). To rule out the possibility that dNxf2 might affect transposons indirectly via Panx stability, we measured transposon expression upon overexpressing λN-Flag-Panx under the dNxf2 mutant background (fig. S3A-E). Consistently, dNxf2 mutant female flies lost transposon control (fig. S3C-D) and were complete sterile despite the overexpression of λN-Flag-Panx (fig. S3E).

The striking phenotypic similarities between dNxf2 and Panx prompted us to test whether these

two proteins interact directly. Therefore, we used yeast two-hybrid (Y2H) assays to determine the interacting regions. The domain architecture of dNxf2 is very similar to that of the canonical RNA export factor, dNxf1/TAP (also known as sbr, Fig. 2A). Both proteins contain leucine-rich repeats (LRR), an RNA recognition motif (RRM), a nuclear transport factor 2 (NTF2)-like domain, and a ubiquitin-associated domain (UBA). Interestingly, Panx only interacts with the UBA domain of dNxf2 (Fig. 2B). This interaction is specific as the UBA domain of dNxf1 showed no binding (Fig. 2B). Surprisingly, however, neither full length nor the NTF2-UBA fragment of dNxf2 could bind Panx (Fig. 2B), suggesting that the UBA domain of dNxf2 might be in a “closed” conformation in the presence of the NTF2 domain. Additionally, the interactions between dNxt1 and the NTF2 domains of either dNxf2 or dNxf1 are significantly weakened in the presence of its UBA domain (Fig. 2C). Since *Drosophila* Nxt1 is absent in yeast, we tested whether dNxt1 might release the UBA domain from the NTF2 domain to permit Panx binding. Indeed, ectopic expression of dNxt1 is sufficient to allow full length dNxf2 to interact with Panx in a yeast-three hybrid assay (Fig. 2D). Next, we mapped the minimum region of Panx down to residues 315-343 (NIR, dNxf2 interacting region) as sufficient for UBA binding (Fig. 2E and fig. S3I). Consistent with the fact that dNxt1 forms a heterodimer with dNxf2(*12*), we found that dNxt1 co-migrates with a fusion protein comprised of $dNxf2^{NTF2\text{-}UBA}$-$(Gly\text{-}Ser)_4$-$Panx^{NIR}$ by size-exclusive chromatography (Fig. 2F), suggesting that Panx, dNxf2, and dNxt1 may exist as a ternary complex. Indeed, purified $Panx^{NIR}$ forms a stable complex with the UBA domain of dNxf2 with a dissociation constant of ~3.2 μM (Fig. 2G). Despite many efforts, we failed to crystalize the $dNxf2^{NTF2}$ domain. Therefore, we determined the crystal structure of $dNxf1^{NTF2}$ in complex with dNxt1 and modelled the binding of $dNxf2^{NTF2}$ to dNxt1 (fig. S4A). Consistent with the Y2H results, $dNxf2^{NTF2}$ maintained most, if not all, residues that interact with dNxt1 (fig. S4A-E).

To further explore the molecular basis of interactions between dNxf2 and Panx, we determined

the structure of the dNxf2-Panx complex (Fig. 3A-D). The structure was solved to a 1.5-Å resolution (Table S1). dNxf2^{UBA} forms a compact three-helix bundle (α1–α3) with a 3_{10}-helix (η1) at the C-terminus (Fig. 3B). The Panx^{NIR} is folded into a long α-helix and lays on the hydrophobic surface formed by α2 and α3 (Fig. 3B-C and fig. S4F). A324, A328, V331, L332, and I335 on Panx interact with V800, F819, F826, F840, L823 and I827 on dNxf2 via hydrophobic interactions (Fig. 3D). Moreover, R321 and R327 on Panx form salt bridges with D837 and E799 on Nxf2^{UBA}, respectively (Fig. 3D). To validate the intermolecular interactions between dNxf2 and Panx, we mutated key residues of the interacting interface (Fig. 3E). While either L823A or D837A single point mutation affected the binding between Panx and dNxf2^{UBA}, the double point mutation of dNxf2^{UBA} F826A/I827A nearly abolished the interactions with Panx in both Y2H and co-immunoprecipitation assays (Fig. 3E-F), highlighting the significant contribution of these residues in Panx binding.

Having demonstrated direct binding between dNxf2 and Panx, we next tested the functional importance of this interaction. We took advantage of a previously described λN/BoxB luciferase reporter system to see if artificial tethering of dNxf2 could lead to repression. Indeed, we observed significant repression upon tethering of a λN-dNxf2 fusion protein (Fig. 3G), unlike that of the negative controls (λN-YFP or GFP-dNxf2 lacking a λN-tag). Similar to Panx, the level of λN-dNxf2 mediated repression appeared to be dosage-dependent, as it correlated with the number of BoxB binding sites (Fig. 3H). Most importantly, the repression is dependent on the presence of the dNxf2 UBA domain (Fig. 3G, dNxf2-ΔUBA).

Our structure provided insight into why dNxf2^{UBA} prefers to bind the silencing factor Panx rather than the FG repeats of the nuclear pore complex (NPC). In contrast to the highly charged surface of the Nxf1-type UBA (i.e. hsNxf1 or scMex67), dNxf2^{UBA} favors hydrophobic binding with Panx (Fig. 3C and fig. S5A-B). Key residues on the interacting interface are highly conserved among

different *Drosophila* species but altered in the Nxf1-type UBA (fig. S5A). On the opposite surface of the Nxf1-type UBA, a hydrophobic pocket is formed to accommodate the FxFG peptide of the NPC (fig. S5C-D). However, this pocket is missing in dNxf2^{UBA} due to a salt bridge formed between K829 and E814 (fig. S5C). Additionally, the bulky side chain of L825 on dNxf2^{UBA} may hinder FG binding (fig. S5C). In contrast, the corresponding amino acids in hsNxf1 (A602) or scMex67 (G583) contain much smaller side chains (fig. S5C-D), therefore, give space for FxFG interactions. Consistent with the structural prediction, dNxf2^{UBA} failed to interact with the FG-repeats of Nup214, a NPC component known to interact with dNxf1^{UBA} (fig. S5E) (*13*). Since two copies of FG binding domains (NTF2 and UBA) are minimally required for proper RNA export(*15*), dNxf2 lacks at least one copy of the FG binding domain (UBA) and thus cannot export RNAs.

The predicted RNA binding domains at the N-terminus of dNxf2 imply that dNxf2 might directly bind to transposon transcripts *in vivo* (Fig. 3A)(*12*). To validate this hypothesis, we performed GoldCLIP/RT-qPCR experiments using an engineered OSC line in which a Halo-tag was fused to the C-terminus of dNxf2 (dNxf2-Halo) (fig. S6A-F)(*16*). GoldCLIP took advantage of the covalent attachment of the Halo-tag to its ligand, affording a denaturing purification of crosslinked protein-RNA complexes(*17*). Strikingly, following UV crosslinking, transposon transcripts (mdg1), but not rp49, remained attached to the dNxf2-Halo fusion protein despite denaturing washes (fig. S6B-C). The association appeared to be direct as it depends on UV crosslinking (fig. S6B-C). Interestingly, the interaction was only observed when both histone H1 and Heterochromatin Protein 1a (HP1a) were depleted by RNAi, but not in the control knockdown (fig. S6B-C). This correlates with the idea that the majority of transposon transcripts remain suppressed in a wildtype background and therefore are not available for dNxf2 binding. Nevertheless, if the downstream silencing factors (H1 and HP1a) were removed, transposon transcripts could accumulate and bind dNxf2 (fig. S6B). In contrast, we failed to detect any CLIP signal on Frogger despite of dramatic up-regulation of its

transcripts upon RNAi (fig. S6D). Since Frogger does not appear to be targeted by Piwi-piRNAs in OSCs(*18*), this result suggests that the binding of dNxf2 to transposon is potentially piRNA-guided. In order to obtain enough material, we performed GoldCLIP-seq experiments using dNxf2-Halo knock-in OSCs depleted of Maelstrom, a piRNA pathway effector component either parallel or downstream of H3K9me3 establishment on transposons(*19*). Consistent with the RT-qPCR results, CLIP-seq demonstrated that dNxf2 binds to Piwi-targeted transposons (Fig. 4A). Collectively, our data strongly argues that Panx and dNxf2/dNxt1 function together as a stable complex to directly suppress transposons that are targeted by Piwi-piRNAs.

Loss of Panx leads to significantly decreased H3K9me3 marks over transposons(*6*, *7*). We next tested if loss of dNxf2 could result in similar phenomena. Since Panx is unstable in the absence of dNxf2 (fig. S2), we performed H3K9me3 ChIP-qPCR assays over several transposons while driving Panx overexpression under a strong promoter (Ubiquitin). H3K9me3 changes seemed rather modest upon removal of dNxf2 (fig. S8B). This result prompted us to look for alternative explanations for dNxf2-mediated silencing. In this regard, dNxf1 was found to be required for transposon silencing in a genome-wide RNAi screen(*10*). Additionally, female flies with mutant alleles of dNxf1 are sterile and have defects in meiotic spindles(*20*), a phenotype reminiscent of core piRNA pathway mutants(*21*, *22*). Hence, we tested if dNxf1 is required for Panx-mediated silencing. Consistent with the RNAi screen data, germline specific depletion of dNxf1 significantly impaired the repression induced by λN-Panx, thereby genetically placing dNxf1 in the Panx-mediated silencing pathway (Fig. 4B). Human Nxf1/TAP has been reported to oligomerize with other NXF family members to regulate RNA export(*23*, *24*). Next we tested whether dNxf2 might interact with dNxf1 directly. Indeed, GFP-tagged dNxf2 can co-immunoprecipitate Halo-tagged dNxf1 from OSC lysates (Fig. 4C). Further domain truncations showed that either NTF2 or UBA domain of dNxf1 is sufficient to interact with the NTF2 domain of dNxf2 (Fig. 4D and fig. S10).

Moreover, GST pull-down assays demonstrated a direct association between dNxf1 and dNxf2 (Fig. 4E and fig. S11). To rule out any indirect or off-target effect of dNxf1 knockdowns, we re-introduced either wild-type dNxf1 or a truncated dNxf1 missing the RNA binding domains (ΔRBD=RRM+LRR) driven by Ubiquitin promoter. As expected, wild-type dNxf1 suppressed the transposon overexpression caused by the shRNA targeting the 5' untranslated region of endogenous dNxf1 (Fig. 4F). Importantly, the truncated dNxf1 lacking the RNA cargo binding domains (ΔRBD) maintained the ability to rescue transposon silencing (Fig. 4F). Because the RBD of dNxf1 is required for RNA export, our results strongly argue against an indirect involvement of dNxf1 in transposon suppression. Next, we sort to directly visualize potential changes in RNA localization by using a rapamycin-induced tethering system (Fig. 4G and fig. S7). GFP mRNAs containing 10 copies of BoxB binding sites tethered with λN-FKBP are mostly localized in the cytoplasm (Fig. 4G). Upon Rapamycin treatment, λN-FKBP dimerizes with FRB-dNxf2 fusion protein, allowing tethering of dNxf2 to the GFP mRNAs. Intriguingly, GFP mRNAs tethered with FRB-dNxf2 start to accumulate at nuclear peripheries (Fig. 4G). The effect is specific to dNxf2 because FRB alone failed to cause any change. Given these properties, we named this multi-protein complex as Pandas (Panx-Nxf2 dependent TAP/p15 silencing). Our data raise the possibility that deterring dNxf1's function in transposon RNA export may be a key event in the process of piRNA-guided silencing (fig. S12).

Like any coding mRNA, if not restrained by Piwi-piRNAs, transposon transcripts would likewise be transported into the cytoplasm by the dNxf1/dNxt1 exporting machinery(*13*). In piRNA-guided TGS, dNxf2/dNxt1 may function together with Panx as a stable complex to counteract this process (fig. S12). As shown by our structural analysis, dNxf2^{UBA} has evolved to lose its ability to bind the NPC (fig. S5). Accordingly, part of dNxf2's silencing function may be hijacking the RNA exporting machinery and repurposing dNxf1 into a "dead-end" complex, hence trapping transposon

228 transcripts within the nucleus (Fig. 4G). In this regard, dNxf1 can localize to nuclear peripheries in
229 which most constitutive heterochromatin resides(*12*, *25*-*27*). Sequestering transposons to these
230 compartments via the Pandas complex may help to establish/maintain their heterochromatic state
231 (fig. S9)(*26*, *27*). Therefore, dNxf2 is likely to function in the Pandas complex to combat transposon
232 expression, at least in part by preventing transposon RNA export (fig. S12).

REFERENCES

1. D. T. Ge, P. D. Zamore, Small RNA-directed silencing: the fly finds its inner fission yeast? *Curr. Biol.* **23**, R318–20 (2013).

2. R. Martienssen, D. Moazed, RNAi and heterochromatin assembly. *Cold Spring Harb Perspect Biol*. **7**, a019323 (2015).

3. B. Czech, G. J. Hannon, One Loop to Rule Them All: The Ping-Pong Cycle and piRNA-Guided Silencing. *Trends Biochem. Sci.* **0** (2016), doi:10.1016/j.tibs.2015.12.008.

4. D. M. Ozata, I. Gainetdinov, A. Zoch, D. X. N. O. X. Carroll, P. D. Zamore, PIWI-interacting RNAs: small RNAs with big functions. *Nat. Rev. Genet.*, 1–20 (2018).

5. I. Gainetdinov, C. Colpan, A. Arif, K. Cecchini, P. D. Zamore, A Single Mechanism of Biogenesis, Initiated and Directed by PIWI Proteins, Explains piRNA Production in Most Animals. *Mol. Cell*. **71**, 775–790.e5 (2018).

6. Y. Yu *et al.*, Panoramix enforces piRNA-dependent cotranscriptional silencing. *Science*. **350**, 339–342 (2015).

7. G. Sienski *et al.*, Silencio/CG9754 connects the Piwi-piRNA complex to the cellular heterochromatin machinery. *Genes Dev.* **29**, 2258–2271 (2015).

8. B. Czech, J. B. Preall, J. McGinn, G. J. Hannon, A transcriptome-wide RNAi screen in the Drosophila ovary reveals factors of the germline piRNA pathway. *Mol. Cell*. **50**, 749–761 (2013).

9. F. Muerdter *et al.*, A genome-wide RNAi screen draws a genetic framework for transposon control and primary piRNA biogenesis in Drosophila. *Mol. Cell*. **50**, 736–748 (2013).

10. D. Handler *et al.*, The genetic makeup of the Drosophila piRNA pathway. *Mol. Cell*. **50**, 762–777 (2013).

11. K. G. Guruharsha *et al.*, A protein complex network of Drosophila melanogaster. *Cell*. **147**, 690–703 (2011).

12. A. Herold, T. Klymenko, E. Izaurralde, NXF1/p15 heterodimers are essential for mRNA nuclear export in Drosophila. *RNA*. **7**, 1768–1780 (2001).

13. J. Katahira, Nuclear export of messenger RNA. *Genes (Basel)*. **6**, 163–184 (2015).

14. F. Port, H.-M. Chen, T. Lee, S. L. Bullock, Optimized CRISPR/Cas tools for efficient germline and somatic genome engineering in Drosophila. *Proc. Natl. Acad. Sci. U.S.A.* **111**, E2967–76 (2014).

15. I. C. Braun, A. Herold, M. Rode, E. Izaurralde, Nuclear export of mRNA by TAP/NXF1 requires two nucleoporin-binding sites but not p15. *Mol. Cell. Biol.* **22**, 5405–5418 (2002).

16. D. Savic *et al.*, CETCh-seq: CRISPR epitope tagging ChIP-seq of DNA-binding proteins. *Genome Res.* **25**, 1581–1589 (2015).

17. J. Gu *et al.*, GoldCLIP: Gel-omitted Ligation-dependent CLIP. *Genomics Proteomics Bioinformatics*. **16**, 136–143 (2018).

18. Y. W. Iwasaki *et al.*, Piwi Modulates Chromatin Accessibility by Regulating Multiple Factors Including Histone H1 to Repress Transposons. *Mol. Cell*. **63**, 408–419 (2016).

19. G. Sienski, D. Dönertas, J. Brennecke, Transcriptional silencing of transposons by Piwi and maelstrom and its impact on chromatin state and gene expression. *Cell*. **151**, 964–980 (2012).

20. E. V. Golubkova *et al.*, Dm nxf1/sbr gene affects the formation of meiotic spindle in female Drosophila melanogaster. *Chromosome Res.* **17**, 833–845 (2009).

21. B. Czech, G. J. Hannon, A Happy 3' Ending to the piRNA Maturation Story. *Cell*. **164**, 838–840 (2016).

22. J. S. Khurana, W. Theurkauf, piRNAs, transposon silencing, and Drosophila germline development. *J. Cell Biol.* **191**, 905–913 (2010).

23. L. H. Matzat, S. Berberoglu, L. Lévesque, Formation of a Tap/NXF1 homotypic complex is mediated through the amino-terminal domain of Tap and enhances interaction with nucleoporins. *Mol. Biol. Cell*. **19**, 327–338 (2008).

24. S. Aibara, J. Katahira, E. Valkov, M. Stewart, The principal mRNA nuclear export factor NXF1:NXT1 forms a symmetric binding platform that facilitates export of retroviral CTE-RNA. *Nucleic Acids Res.* **43**, 1883–1893 (2015).

25. D. E. Kerkow *et al.*, The structure of the NXF2/NXT1 heterodimeric complex reveals the combined specificity and versatility of the NTF2-like fold. *J. Mol. Biol.* **415**, 649–665 (2012).

26. B. van Steensel, A. S. Belmont, Lamina-Associated Domains: Links with Chromosome Architecture, Heterochromatin, and Gene Repression. *Cell*. **169**, 780–791 (2017).

27. B. D. Towbin, P. Meister, S. M. Gasser, The nuclear envelope--a scaffold for silencing? *Curr. Opin. Genet. Dev.* **19**, 180–186 (2009).

28. K. Saito *et al.*, A regulatory circuit for piwi by the large Maf gene traffic jam in Drosophila. *Nature*. **461**, 1296–1299 (2009).

29. C. D. Armour *et al.*, Digital transcriptome profiling using selective hexamer priming for cDNA synthesis. *Nat. Methods*. **6**, 647–649 (2009).

30. M. Martin, Cutadapt removes adapter sequences from high-throughput sequencing reads. *EMBnet.journal*. **17**, 10–12 (2011).

31. A. Dobin *et al.*, STAR: ultrafast universal RNA-seq aligner. *Bioinformatics*. **29**, 15–21 (2013).

32. M. E. Ritchie *et al.*, limma powers differential expression analyses for RNA-sequencing and microarray studies. *Nucleic Acids Res.* **43**, e47–e47 (2015).

33. E. Radion *et al.*, Key role of piRNAs in telomeric chromatin maintenance and telomere

nuclear positioning in Drosophila germline. *Epigenetics Chromatin*. **11**, 40 (2018).

34. P. D. Adams *et al.*, PHENIX: a comprehensive Python-based system for macromolecular structure solution. *Acta Crystallogr. D Biol. Crystallogr.* **66**, 213–221 (2010).

35. P. Emsley, K. Cowtan, Coot: model-building tools for molecular graphics. *Acta Crystallogr. D Biol. Crystallogr.* **60**, 2126–2132 (2004).

36. A. Waterhouse *et al.*, SWISS-MODEL: homology modelling of protein structures and complexes. *Nucleic Acids Res.* **46**, W296–W303 (2018).

37. H. McWilliam *et al.*, Analysis Tool Web Services from the EMBL-EBI. *Nucleic Acids Res.* **41**, W597–600 (2013).

38. X. Robert, P. Gouet, Deciphering key features in protein structures with the new ENDscript server. *Nucleic Acids Res.* **42**, W320–4 (2014).

Figure 1. dNxf2 functions as a cofactor of Panx in the piRNA pathway.

A, Western blots showing co-immunoprecipitation of endogenous dNxf2 with GFP-Panx from ovary lysates. Two different rabbit polyclonal monospecific dNxf2 (dNxf2-N and dNxf2-C) antibodies were used to detect endogenous dNxf2. **B**, Halo-ligand staining and western blots showing co-immunoprecipitation of endogenous Panx with dNxf2-Halo driven by the endogenous dNxf2 promoter from OSC lysates. A rabbit polyclonal monospecific Panx antibody was used to detect endogenous Panx. Left panel shows depletion of dNxf2-Halo proteins in the unbound sample by Halo beads, and the anti-Tubulin blots serve as loading controls; Right panel shows endogenous Panx proteins. **C**, The effects of germline (*nanos*-GAL4) knockdown of the indicated genes on Renilla-normalized Firefly luciferase activity of the reporter while tethering λN-Panx. For comparison, the relative value of the attp2 control was used for normalization. Data show mean ± s.d. (n = 15; *P = 1.41387E-07). **D**, Comparison of steady-state RNA levels are shown as reads per million (rpm) mapping to the sense strand of each transposon consensus from the *nanos*-GAL4 driven knockdown for dNxf2 (Y axis) versus control (X axis). Dashed lines indicate two-fold changes. The average of two replicates is shown. KD = knockdown. Red dots indicate transposon elements with significant changes. **E**, Comparison of steady-state RNA levels (RNA-seq; shown as RPM) mapping to the sense strands of each transposon consensus from the *nanos*-GAL4 driven knockdowns of the indicated genes. Red dots indicate transposon elements with significant changes from **D**. **F**, Heat map displaying steady-state RNA levels (RNA-seq) as reads per million (rpm) for top 70 detected transposons from the *nanos*-GAL4 driven knockdowns of the indicated genes in a blue-white scale.

Figure 2. The UBA domain of dNxf2 interacts with Panx directly.

A, Domain architectures of Panx, dNxf2, dNxf1, and dNxt1 are shown. Numbers above the diagrams correspond to amino acid residues of each protein. Domain names are abbreviated within respective colored region. **B-E**, Y2H assays mapping the interacting regions between *Drosophila* Nxf1/2 and Panx or dNxt1. Interactions were determined by either measuring the beta-galactosidase activity produced by the reporter gene or growth on YSD media lacking the indicated essential amino acid or Uracil. Data are averages of three independent experiments (n=3). Proteins or fragments shown above the dashed line are used as preys in the assays. **B**, Y2H assays mapping regions of *Drosophila* Nxf1/2 that interact with Panx. **C**, Y2H assays mapping regions of *Drosophila* Nxf1/2 that interact with dNxt. **D**, Yeast three hybrid determining the requirement of dNxt1 for Nxf2:Panx interaction. **E**, Y2H assays mapping minimum regions of Panx that interact with $dNxf2^{UBA}$. **F**, Left panel shows the size exclusive chromatography profile of the NTF2 and UBA domains of dNxf2 forming heterodimers with dNxt1 and $Panx^{NIR}$ in solution, respectively. A dNxf2 fragment spanning the NTF2 and UBA domains that is covalently linked to $Panx^{NIR}$ forms a stable complex with dNxt1. Right panel, SDS-PAGE shows the components of the peak in the elution profile. Color schemes used for the three complexes are indicated in the key. **G**, Quantification of the dissociation constant for the interaction between $dNxf2^{UBA}$ and $Panx^{NIR}$ as measured by an isothermal titration calorimetry assay.

Figure 3. Structure of dNxf2^{UBA} in complex with Panx^{NIR}.

A, Schematic of interacting region between dNxf2 and Panx. Numbers above or below the diagrams correspond to amino acid residues of dNxf2 or Panx, respectively. Domain names are abbreviated within respective colored region. NIR, dNxf2 interacting region. **B**, Left, cartoon representation of dNxf2^{UBA} in complex with Panx^{NIR}. The dNxf2^{UBA} and Panx^{NIR} fragment are colored in wheat and teal, respectively. Right, a view rotated 90° around the vertical axis. **C**, Electrostatic potential analysis showing the Panx-binding surface of dNxf2^{UBA}. Panx^{NIR} is shown in cartoon mode. **D**, A detailed view showing the interactions between dNxf2^{UBA} and Panx^{NIR}. Key residues involved in binding are shown in sticks. Close-up views of hydrophobic interactions between dNxf2^{UBA} and Panx^{NIR} are shown on the right. **E**, Y2H assays measuring the binding of wild-type or mutant dNxf2^{UBA} with Panx^{NIR}. Mutations of key residues are indicated along the bars. **F**, Western blots and Halo-ligand staining showing co-immunoprecipitation of GFP-tagged Panx or its NIR deletion mutant (ΔNIR) with Halo-tagged dNxf2 or its F826A/I827A double mutant from OSC cells. GFP serves as a negative control. **G**, Effects of the indicated λN fusion proteins or a non-tethering control (GFP-dNxf2) on luciferase activity of the reporters integrated into the attP2 landing site. Data show mean ± s.d. (n = 15; *P = 1.41387E-07). **H**, The effects of λN-dNxf2 tethering on luciferase activity of reporters with increasing number of BoxB sites. All reporters are integrated into the same genomic locus (attP2 landing site). Fold repression is calculated as total protein-normalized Firefly luciferase luminescent values of the control (no tethering) divided by that of the indicated experiments. Data show mean ± s.d. (n = 15; *P = 1.41387E-07).

Figure 4. The Pandas complex is required for piRNA-guided transposon silencing.

A, Comparison of GoldCLIP-seq are shown as reads per million (rpm) mapping to the sense strand of each transposon consensus for Maelstrom (*X* axis) versus a LacZ control knockdown (*Y* axis). A mammalian spike-in was used to normalize different samples. Dashed lines indicate two-fold changes. The pooled reads from two replicates are shown. Red dots indicate Piwi-targeted transposons, blue dots indicate H1-dependent transposons and green dots indicate other transposons. B, The effects of germline specific knockdown (nanos-GAL4) of the indicated genes on Renilla-normalized Firefly luciferase activity of the reporter while tethering λN-Panx. For comparison, the results from Fig. 1C (Egg, attp2 and Zuc) were shown here again. Data show mean ± s.d. (n = 15; *P = 1.41387E-07). **C**, Western blots and Halo-ligand staining showing co-immunoprecipitation of GFP-tagged dNxf2 with Halo-tagged dNxf1 from OSC cells. ΔNTF2, Halo-dNxf1 lacking the NTF2 domain, and GFP serves as a negative control. **D**, Western blots and Halo-ligand staining showing co-immunoprecipitation of Halo-tagged dNxf2-NTF2 domain with different domain truncations of GFP-tagged dNxf1 from OSC cells. ΔRBD, dNxf1 lacking the N-terminus RRM and LRR domains; GFP serves as a negative control. **E**, SDS-PAGE showing pulldown results of the Nxf2$^{NTF2+UBA}$-(GS)4-Panx^{NIR}/dNxt1 complex by either GST-tagged dNxf1-NTF2 or dNxf1-(NTF2+UBA) respectively, compared to a GST control. **F**, RT-qPCR results showing the effects of germline (*nanos*-GAL4) knockdown of the indicated genes in the presence or absence of different transgenes. Fold changes are calculated as rp49-normalized RNA levels divided by that of the corresponding controls. Mean values ± s.d. from 3 independent experiments are shown. **G**, SIM super-resolution microscopy of RNA FISH detected by HCR2.0. Data showing the comparison of the localizations of the reporter mRNAs tethered with λN-FKBP, upon transient recruitment of either FRB-dNxf2 or FRB alone when treated with rapamycin for 2 hours to induce FKBP:FRB dimerization. Top panel, RNA signal (red) with DAPI staining; middle, DAPI staining (blue); bottom, RanGAP-GFP fusion protein (green) were shown. The scale bar represent 5 μM in length.

Figure 1

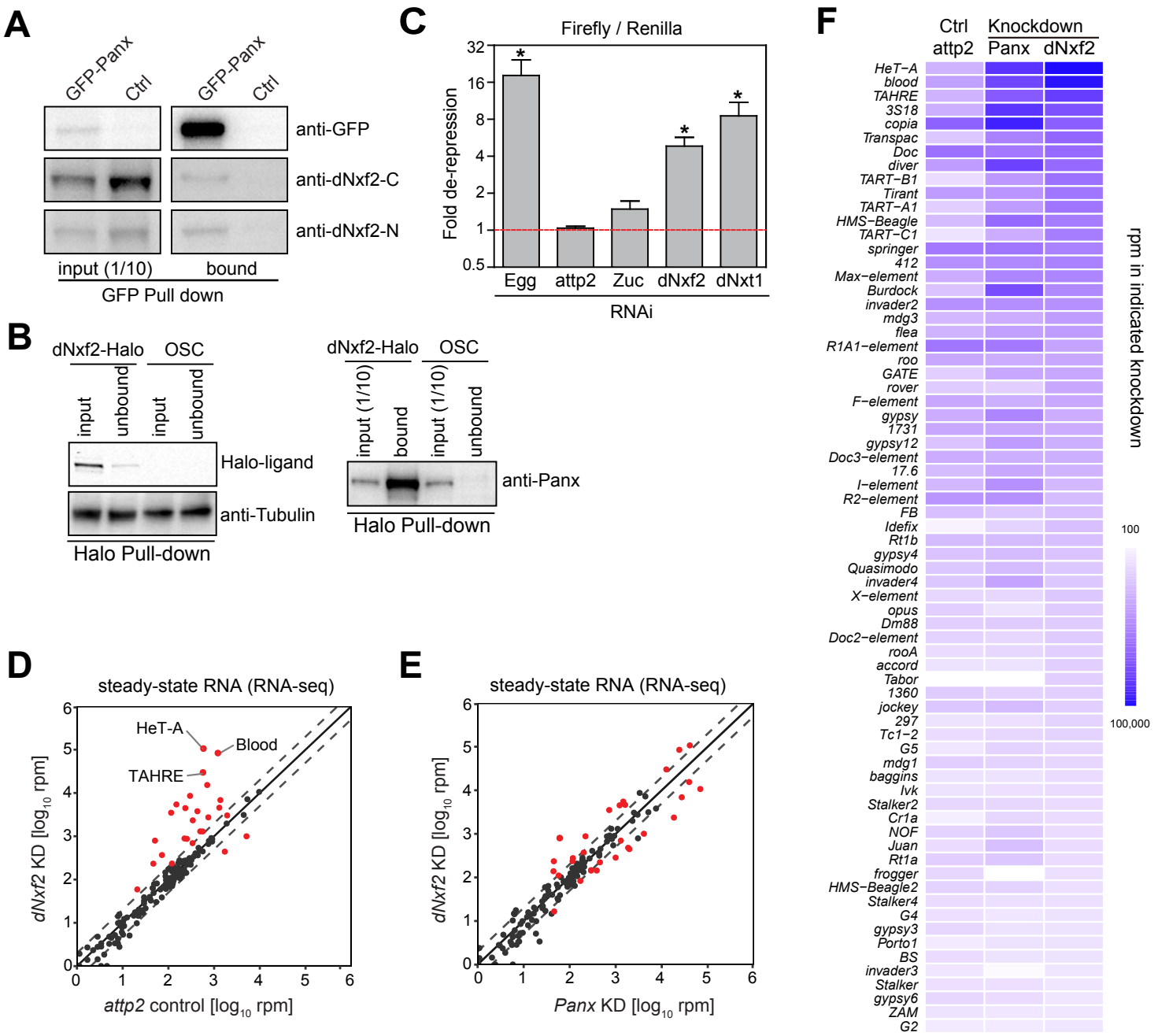

Figure 2

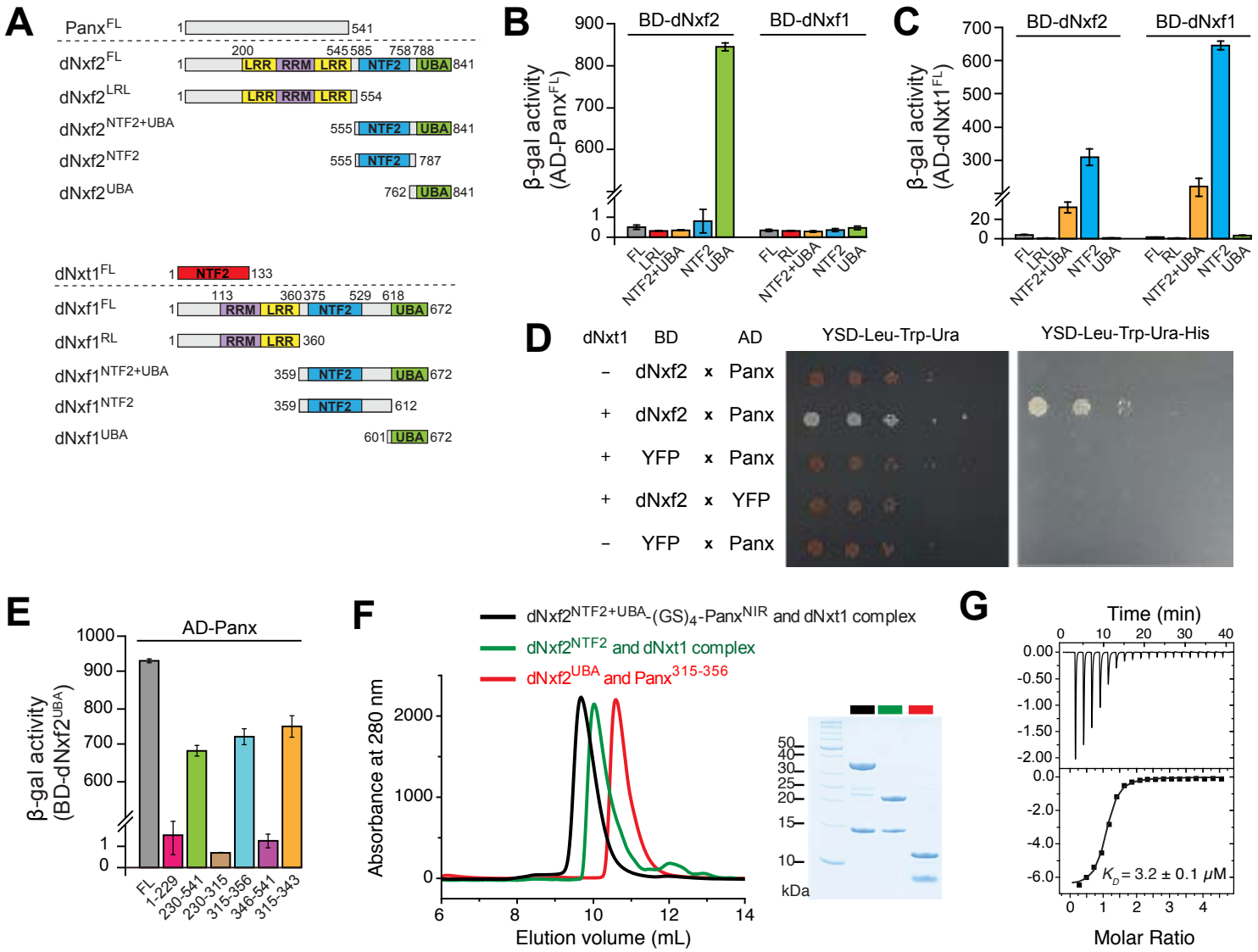

Figure 3

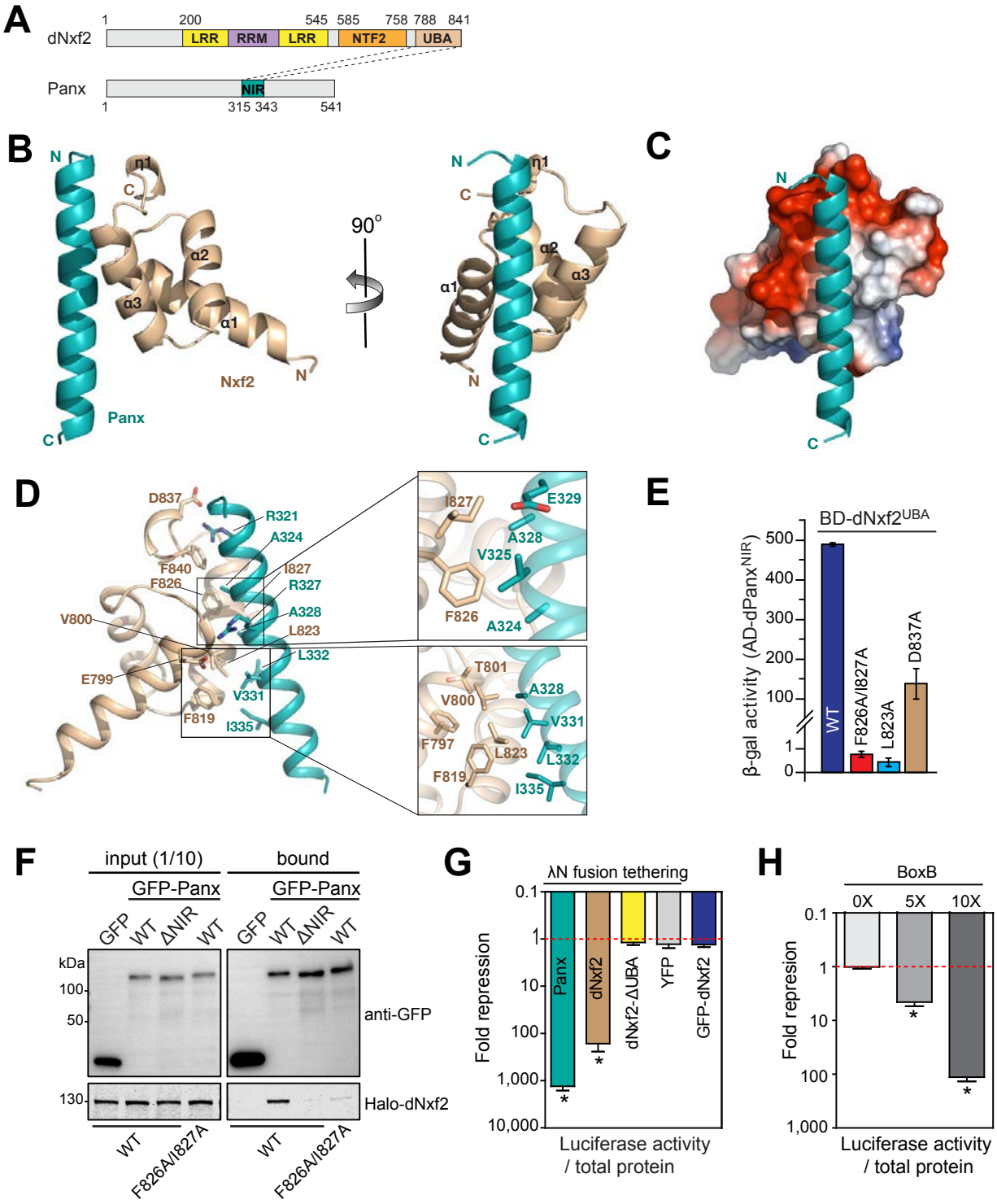

Figure 4